

Diagnosis of Dyslexia Based on 3D Shape Analysis of the Brain Cortex

No Author Given

No Institute Given

Abstract. To discriminate more accurately between dyslexic and normal brains, we detect the brain cortex variability through a spherical harmonic analysis that represents a 3D surface supported by the unit sphere having a linear combination of special basis functions, called spherical harmonics (SHs). The proposed 3D shape analysis is carried out in five steps: (i) 3D brain cortex segmentation, with a deformable 3D boundary, controlled by two probabilistic visual appearance models (the learned prior model and the estimated current appearance model); (ii) 3D Delaunay triangulation to construct a 3D mesh model of the brain cortex surface; (iii) mapping this model to the unit sphere; (iv) computing the SHs for the surface, and (v) determining the number of the SHs to delineate the brain cortex. We describe the brain shape complexity with a new shape index, the estimated number of the SHs, and use it for the K -nearest classification into the normal and dyslexic brains. Initial experiments suggest that our shape index is a promising supplement to the current dyslexia diagnostic techniques.

1 Introduction

Developmental brain disorders are among the most interesting and challenging research areas in modern neuroscience. Dyslexia is an extremely complicated example of such disorders that severely impairs the learning abilities of children. It is characterized by substandard reading skills, which remain unaccounted for after considering an individual's age, overall intelligence, and education [1]. Dyslexia affects many aspects of the brain, so improved diagnostic methods are necessary.

Recent advances in neuro-imaging suggest new non-invasive methods for automatic dyslexia detection by revealing the differences between quantitative characteristics of normal and dyslexic brains. Casanova et al. [2] and Eliez et al. [3] demonstrated a reduction in the gyral index (i.e., the ratio of the pial surface's contour to the convex hull of the brain surface) of dyslexic patients. These recent advances suggest that any gyral abnormality resides in the brain folding rather than the thickness of the cortex.

In addition to the reduction in gyral index, alterations of different brain structures have been found in dyslexic individuals as opposed to normal ones. For example, MRI studies have shown abnormality in the corpus callosum (CC) of dyslexic brains. Plessen et al. [4] computed the mean shape of both dyslexic and normal CCs and noticed that the CC body length can discriminate between the dyslexic and normal subjects. Our recent study [5] reported significant differences in all anatomical divisions, i.e. splenium, rostrum, genu and body of dyslexic CCs by applying a 3D shape analysis of the corpus callosum surface. Another brain abnormality is the altered density of grey

matter in specific regions of dyslexic brains. Different studies (e.g., [3, 6]) analyzed the grey matter regions using a voxel-based morphometry (VBM) approach. This approach normalizes the brains stereotactically to a common space (e.g., an atlas with predefined anatomic subregions) and uses voxel statistics to identify the anatomic brain regions containing altered grey matter densities. Unfortunately, this approach provides a volumetric measure of the overall gross change of the brain structure and does not provide a robust detection measure for the shape of the brain. Analysis of cerebral white matter (CWM) changes for dyslexic subjects has been proposed (e.g., in [7, 8]). Klingberg et al. [7] and Niogi et al. [8] attempted to analyze the relation of the CWM to dyslexia by analyzing the fractional anisotropy (FA) score extracted from diffusion tensor imaging (DTI). The FA is a micro-structural feature that reflects how the diffusion within a voxel depends on orientation. To compute the FA score, Klingberg et al. [7] applied a voxel-based approach that is based on the Statistical Parametric Mapping software package to spatially smooth and normalize brains before analyzing the FA values. Niogi et al. [8] determined a region of interest either manually or semi-automatically using manual user-selected seed pixels to analyze the resulting FA scores. The aforementioned detection methods have the following limitations: (i) they are subject to the influence of spatial smoothing and spatial registration associated with the voxel-based analysis, and (ii) they are only capable of detecting gross change because of their volumetric approach and cannot account for the detailed change in the gyrifications of the cortex.

Instead of examining the volumetric changes in individual brain structures, our recent diagnosis system [9] quantified differences between the shape of CWM gyrifications for dyslexic and normal subjects by analyzing 3D MRI brain images and classified the subjects based on the CWM gyrifications thickness. This paper attempts to analyze and quantify differences between the whole 3D brain cortex shapes for dyslexic and normal subjects in order to discriminate between them more robustly as demonstrated in the experimental section.

2 3D shape analysis framework

The proposed analysis begins with brain cortex segmentation from 3D MR images using a deformable 3D boundary controlled by two probabilistic visual appearance models (the learned prior model and the estimated current appearance model). Then a 3D mesh model of the cortex surface is mapped to a unit sphere, and approximated by a linear combination of spherical harmonics (SHs). The number of SHs used in reconstruction yields a desired approximation accuracy that can be used as a new shape index to describe the complexity of the brain shape. Then a K -nearest classifier separates the dyslexic and normal subjects using their shape indexes.

2.1 Brain cortex segmentation

The accurate cortex segmentation from 3D T2-MR images is a challenging problem, because there are no clear differences between intensities in the cortex and the surrounding organs. To overcome this problem, we use a conventional 3D parametric deformable boundary [10] but control its evolution with two probabilistic visual appearance models, a learned cortex appearance prior model and a current appearance model of the image to be segmented. The prior is a 3D Markov-Gibbs random field (MGRF) model of the cortex intensities with translation- and rotation-invariant pairwise voxel interaction, being learned analytically from training data in accord with [11, 12]. The current

appearance is modeled by a mixed marginal distribution of the voxel intensities in both the brain cortex and surrounding tissues. To extract the voxel-wise model of the current cortex appearance, the mixture is precisely approximated with a linear combination of discrete Gaussians (LCDG) [13] and automatically separated into the cortex and background LCDG models. Fig. 1 demonstrates the results of our cortex segmentation, and Fig. 2 visualizes our results in 3D. The Gibbs energies for each of the brain cortex voxel are higher than for any other brain tissues, making the proposed approach very accurate (our segmentation error with respect to the radiologist’s ”ground truth” is about 2.3%). For more details about the segmentation model and for a comparison with other approaches see [9].

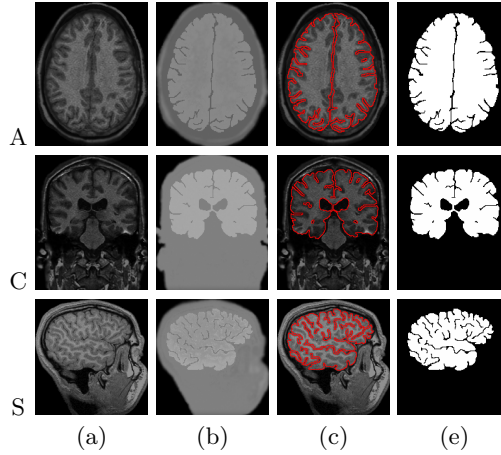


Fig. 1. 3D brain cortex segmentation projected onto 2D axial (A), coronal (C), and sagittal (S) planes for visualization: 2D slices of the original T2-MRI images (a), pixel-wise Gibbs energies (b), our segmentation (c), and the radiologist’s segmentation (d).

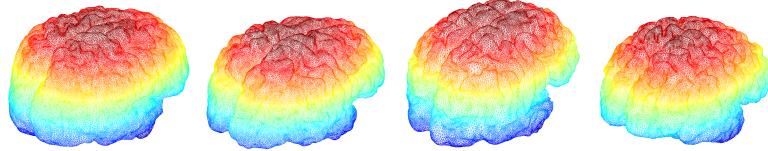


Fig. 2. 3D visualizations of the segmented cortex images shown for four different subjects.

2.2 Spherical harmonics (SHs) shape analysis

Spectral SH analysis [14] considers a set of 3D surface data as a linear combination of specific basis functions. In our case, the surface of the segmented brain cortex is approximated first by a Delaunay triangulated 3D mesh (see Fig. 3) constructed using an algorithm based on Fang and Boas [15]. Secondly, the brain cortex surface for each subject is mapped to the SH decomposition to a unit sphere. We propose a novel mapping approach, called “*Attraction-Repulsion*” that calls for all the mesh nodes to meet two conditions: (i) the unit distance of each node from the brain cortex center as shown in Fig. 4. , and (ii) an equal distance of each node from all of its nearest neighbors as shown in Fig. 5.

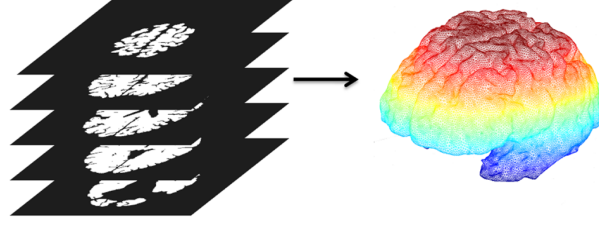


Fig. 3. Generating a 3D mesh for the brain cortex surface from a stack of successive segmented 2D T2-MR slices.

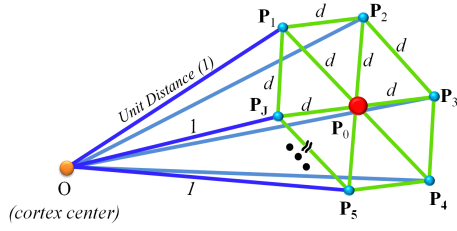


Fig. 4. 3D illustration of the unit distance from all surface nodes to the center of the brain cortex.

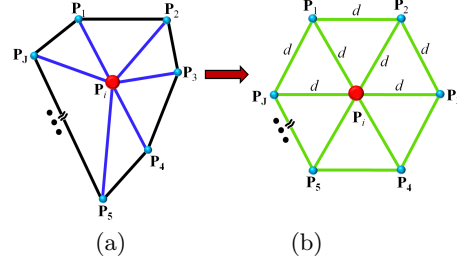


Fig. 5. 2D illustration of the neighbors rearrangement: (a) initial vs. (b) final equidistant locations in all the directions.

To detail our Attraction-Repulsion Algorithm (see its summary in Algorithm 1), let τ denote the iteration index, I be the total number of the mesh nodes (in all the experiments below $I = 48962$ nodes), and $\mathbf{P}_{\tau,i}$ be the Cartesian coordinates of the surface node i at iteration τ ; $i = 1, \dots, I$. Let J be the number of the neighbors for a mesh node (see e.g., Fig. 5) and $d_{\tau,ij}$ denote the Euclidean distance between the surface nodes i and j at iteration τ (as shown in Fig. 5(b)), where $i = 1, \dots, I$ and $j = 1, \dots, J$. Let $\Delta_{\tau,ji} = \mathbf{P}_{\tau,j} - \mathbf{P}_{\tau,i}$ denote the displacement between the nodes j and i at iteration τ . Let $C_{A,1}$, $C_{A,2}$, C_R be the attraction and repulsion constants, respectively, that control the displacement of each surface node.

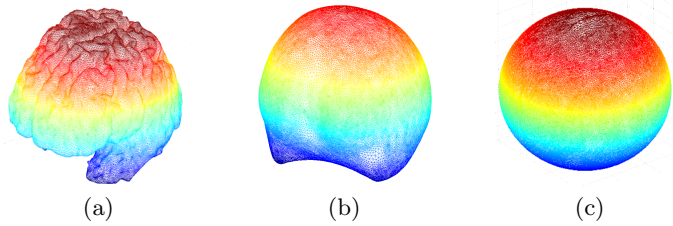


Fig. 6. Brain cortex mesh (a), its smoothed version (b), and the Attraction-Repulsion mapping to the unit sphere (c).

The starting attraction step of the proposed mapping centers each node \mathbf{P}_i ; $i = 1, \dots, I$, with respect to its neighbors by adjusting iteratively its location:

$$\mathbf{P}'_{\tau,i} = \mathbf{P}_{\tau,i} + C_{A,1} \sum_{j=1; j \neq i}^J \Delta_{\tau,ji} d_{\tau,ji}^2 + C_{A,2} \frac{\Delta_{\tau,ji}}{d_{\tau,ji}} \quad (1)$$

Algorithm 1: Attraction-Repulsion Algorithm

Initialization

- Construct the 3D brain cortex mesh (Fig. 6,a).
- Smooth the mesh using Laplacian filtering (Fig. 6,b).
- Initialize the mapping of the smoothed mesh to the unit sphere.

Repeat

- **For** $i = 1 \rightarrow I$
 - **Attraction:**
 - * Select a node to process.
 - * Update the node using Eq. (1)
 - **Repulsion:**
 - * Update the node using Eq. (2).
- **End** (all nodes in the mesh are shifted and back-projected onto the unit sphere).

While changes in the node positions occur (Fig. 6,c).

where the factor $C_{A,2}$ keeps the tightly packed nodes from collision and also pushes the adjusted nodes away from their neighbors if a certain neighbor is much closer than the others.

The subsequent repulsion step inflates the whole mesh by pushing all the nodes outward to become evenly spaced after their final back-projection onto the unit sphere along the rays from the center of the sphere. To ensure that the nodes that have not been shifted will not collide with the altered node, the location of each node \mathbf{P}_i ; $i = 1, \dots, I$, is updated before the following back-projection:

$$\mathbf{P}_{\tau+1,i}^\circ = \mathbf{P}'_{\tau,i} + \frac{C_R}{2I} \sum_{j=1; j \neq i}^I \left(\frac{\Delta_{\tau,ji}}{|\Delta_{\tau,ji}|^2} \right) \quad (2)$$

where a repulsion constant C_R controls the displacement of each surface node and establishes a balance between the processing time and accuracy (e.g., a smaller C_R values guarantees that the node faces will not become crossed during the iterations at the expense of the increased processing time). All the experiments below are obtained with $0.4 \leq C_R \leq 0.6$.

The original brain cortex, mapped to the unit sphere using the proposed Attraction-Repulsion algorithm, is approximated by a linear combination of SHs. The lower-order harmonics are sufficient to represent more generic shape information, while the higher-order harmonics contain the fine details of the shape. The SHs are generated by solving an isotropic heat equation for the cortex surface on the unit sphere. Let $S : \mathbf{M} \rightarrow \mathbf{U}$ denote the mapping of a cortical mesh \mathbf{M} to the unit sphere \mathbf{U} . Each node $\mathbf{P} = (x, y, z) \in \mathbf{M}$ mapped to the spherical position $\mathbf{u} = S(\mathbf{P})$ is represented by the spherical coordinates $\mathbf{u} = (\sin \theta \cos \varphi, \sin \theta \sin \varphi, \cos \theta)$ where $\theta \in [0, \pi]$ and $\varphi \in [0, 2\pi)$ are the polar and azimuth angles, respectively. The SH $Y_{\alpha\beta}$ of degree α and order β is defined as [16]:

$$Y_{\alpha\beta} = \begin{cases} c_{\alpha\beta} G_{\alpha}^{|\beta|} \cos \theta \sin(|\beta|\varphi) & -\alpha \leq \beta \leq -1 \\ \frac{c_{\alpha\beta}}{\sqrt{2}} G_{\alpha}^{|\beta|} \cos \theta & \beta = 0 \\ c_{\alpha\beta} G_{\alpha}^{|\beta|} \cos \theta \cos(|\beta|\varphi) & 1 \leq \beta \leq \alpha \end{cases} \quad (3)$$

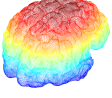
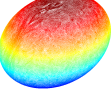
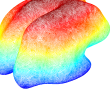
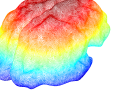
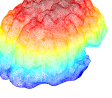
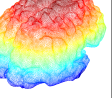
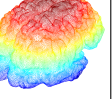
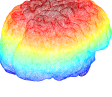
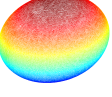
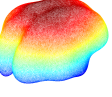
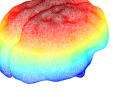
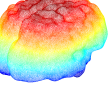
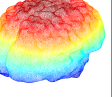
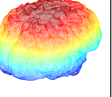
| | Original | 1 SH | 10 SHs | 20 SHs | 30 SHs | 40 SHs | 60 SHs |
|---|---|---|---|---|--|---|---|
| C |  |  |  |  |  |  |  |
| D |  |  |  |  |  |  |  |

Fig. 7. Approximation of the 3D brain cortex shape for control (C) and dyslexic subjects (D).

where $c_{\alpha\beta} = \left(\frac{2\alpha+1}{2\pi} \frac{(\alpha-|\beta|)!}{(\alpha+|\beta|)!} \right)^{\frac{1}{2}}$ and $G_{\alpha}^{|\beta|}$ is the associated Legendre polynomial of degree α and order β . For the fixed α , the polynomials G_{α}^{β} are orthogonal over the range $[-1, 1]$. As shown in [16], the Legendre polynomials are an effective means of calculating SHs, and this is the main motivation behind their use in this work.

Finally, the brain cortex is reconstructed from the SHs of Eq. (3). In the case of the SHs expansion, the standard least-square fitting does not model accurately the 3D shape of the brain cortex and can miss some of the shape details that discriminate between the dyslexic and normal brains. To circumvent this problem, we used the iterative residual fitting by Shen et al. [17] that accurately approximates 3D gyrifications for dyslexic and normal brain cortices. As demonstrated in Fig. 7, the reconstruction using SHs shows significantly less change for dyslexic subjects when compared to the control subjects as the number of SHs increases.

2.3 Quantitative brain cortex shape analysis

Our main hypothesis is that the brain cortex gyral frequency for dyslexic subjects is lower than for the control ones as shown in Fig. 7, so that less SHs have to be used for accurate approximation of the brain cortex gyrifications. Therefore, the number of the SHs, after which there is no significant changes in the approximations, can be used as a new shape index quantifying the cortex complexity of both the dyslexic and normal brains. Due to the unit sphere mapping, the original brain cortex mesh for each subject is inherently aligned with the mesh for the approximate shape, and the sum of the Euclidean distances between the corresponding nodes gives the total error between both of the mesh models. As shown in Fig. 8, the total error curves for the increasing number \mathcal{K} of the SHs can be used as a discriminatory feature to differentiate between the dyslexic and control subjects.

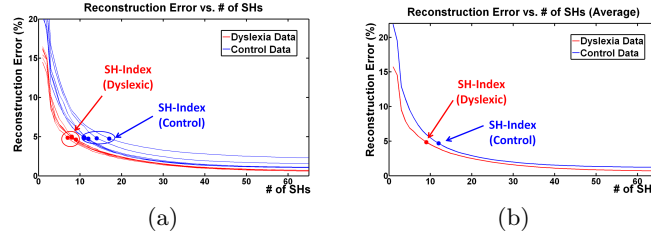


Fig. 8. Estimation of the individual (a) and average (b) shape indices for the total cortex approximation error for dyslexic and control subjects.

3 Experimental Results and Conclusions

The proposed approach has been tested on *in-vivo* data that had been collected from 30 subjects (16 dyslexic subjects of age 18 ± 40 years and 14 control subjects of age 18 ± 40 years). The subjects were scanned using a 1.5 Tesla GE MRI system with voxel resolution of $0.9375 \times 0.9375 \times 1.5 \text{ mm}^3$ using a T2 weighted imaging sequence protocol. The "ground truth" diagnosis used to evaluate the classification accuracy for each patient was given by five medical experts.

The training subset for classification was arbitrarily selected among all 30 subjects. The classification accuracy of the k -nearest classifier for both the training and test subjects was evaluated using the χ^2 -test at three confidence levels, 85, 90, and 95%, in order to examine significant differences in the estimated SH index. As expected, the 85% and 90% confidence levels yielded the best results and correctly classified 16 out of 16 dyslexic subjects (a 100% accuracy) and 14 out of 14 control subjects (a 100% accuracy). The 95% confidence level obviously gives smaller accuracy rates for both the groups, accurately identifying 15 out of 16 dyslexic subjects (93.7%) and 12 out of 14 control subjects (85.7%). The accuracy of the traditional volumetric approach [3] is 7 out of 16 dyslexic subjects (43.75%), and 9 out of 14 control subjects (64.29%) at the 85% confidence level. At a 95% confidence level our approach is more accurate than the traditional approach which uses only an 85% confidence level. These results highlight the advantage of this proposed diagnostic tool.

Another way to measure and test the performance of the system is to compute the receiver operating characteristic (ROC). Each point on the graph is generated by using a different cut point (classification threshold). Figure 9 shows the ROC curve of the two approaches; our proposed centerline based diagnostic approach and the traditional volumetric based diagnostic approach [3]. It is clear from the data in Fig 9 that the area under the ROC curve of our present approach is much larger ($Az = 0.9343$) than the area under the ROC curve for the volumetric based diagnostic approach [3] ($Az = 0.6574$).

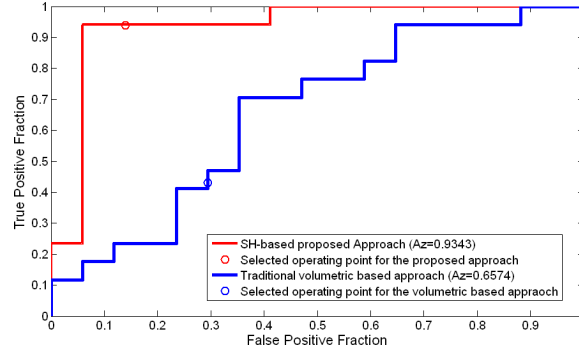


Fig. 9. The ROC curves for the proposed centerline based diagnostic approach and the traditional volumetric based diagnostic approach [3]. Note that 'Az' stands for the area under the curve.

These preliminary results show that the proposed 3D brain cortex shape analysis method is capable of accurately discriminating between dyslexic and control subjects. Our proposal substantially differs from known diagnostic techniques that exploit only volumetric descriptions of different brain structures and are therefore much more

sensitive to the selection of ages and to segmentation errors. We derive our efficient quantitative classification feature from the analysis of the entire 3D cortex shape. Our experiments demonstrate that the proposed general geometric feature of cortex gyrifications has shown statistically significant differences for the control and dyslexic subjects under consideration. In the future, we plan to investigate additional brain structures in order to quantitatively characterize their temporal development and to track the change in a dyslexic brain. To validate and possibly modify the proposed approach, we will test it on larger data sets with known ground truths (i.e., the doctors' diagnoses).

References

1. K. Pugh, W. Mencl, A. Jenner, et al., "Functional neuroimaging studies of reading and reading disability (developmental dyslexia)", *Mental Retardation and Developmental Disabilities Research Reviews*, 2000, 6: 61-79.
2. M. Casanova, J. Araque and J. Giedd, "Reduced brain size and gyrification in the brains of dyslexic patients", *Journal of Child Neurology*, 2004, 9(4):275-281.
3. S. Eliez, J. Rumsey, J. Giedd, et al., "Morphological alteration of temporal lobe gray matter in dyslexia: an MRI study," *J. Child Psychology and Psychiatry*, 2000, 41(5):637-644.
4. K. von Plessen, A. Lundervold, et al., "Less developed corpus callosum in dyslexic subjects - A structural MRI study", *Neuropsychologia*, 2002, 40:1035-1044.
5. Anonymous.
6. G. Silani, U. Frith, et al., "Brain abnormalities underlying altered activation in dyslexia: a voxel based morphometry study", *Brain*, 2005, 128:2453-2461.
7. T. Klingberg, M. Hedehus, et al., "Microstructure of Temporo-Parietal White Matter as a Basis for Reading Ability: Evidence from Diffusion Tensor Magnetic Resonance Imaging", *Neuron*, 2000, 25:493-500.
8. S. Niogi and B. McCandliss, "Left lateralized white matter microstructure accounts for individual differences in reading ability and disability", *Neuropsychologia*, 2006, 44:2178-2188.
9. Anonymous.
10. M. Kass, A. Witkin, and D. Terzopoulos, "Snakes: Active contour models", *Int. J. of Computer Vision*, 1987, 1:321-331.
11. G. Gimel'farb, *Image Textures and Gibbs Random Fields*, Kluwer Academic, 1999.
12. G. Gimel'farb and D. Zhou, "Texture analysis by accurate identification of a generic Markov Gibbs Model", in *Applied Pattern Recognition (Studies in Computational Intelligence 91)*. Berlin:Springer, 2008, 221-245.
13. Anonymous.
14. M. K. Chung, L. Shen, K. M. Dalton, et al., "Weighted Fourier series representation and its application to quantifying the amount of gray matter", *IEEE Trans. on Med. Imaging*, 2007, 26:566-581.
15. Q. Fang and D. Boas, "Tetrahedral mesh generation from volumetric binary and gray-scale images", in *Proc. IEEE Int. Symp. on Biomedical Imaging: From Nano to Macro (ISBI'09)*, Boston, MA, USA, June 28-July 1, 2009, 1142-1145.
16. R. Courant and D. Hilbert, *Methods of Mathematical Physics Vol. I*, London: Interscience, 1953.
17. L. Shen and M. K. Chung, "Large-scale modeling of parametric surfaces using spherical harmonics", in *Proc. 3rd Int. Symp. 3D Data Process. Visualiz. Transmission (3DPVT)*, Chapel Hill, NC, USA, June 14-16, 2006, 294-301.